

See discussions, stats, and author profiles for this publication at: <https://www.researchgate.net/publication/263962124>

The Flexible Surface Revisited: Adsorbate-Induced Reconstruction, Homocoupling, and Sonogashira Cross-Coupling on the Au(100) Surface

ARTICLE *in* THE JOURNAL OF PHYSICAL CHEMISTRY C · MAY 2014

Impact Factor: 4.77 · DOI: 10.1021/jp501321u

CITATIONS

4

READS

51

6 AUTHORS, INCLUDING:



[Carlos Sánchez-Sánchez](#)

Empa - Swiss Federal Laboratories for Materi...

23 PUBLICATIONS 256 CITATIONS

[SEE PROFILE](#)



[Francisco Yubero](#)

Spanish National Research Council

184 PUBLICATIONS 2,552 CITATIONS

[SEE PROFILE](#)



[Agustín R. González-Elipe](#)

Spanish National Research Council

434 PUBLICATIONS 7,306 CITATIONS

[SEE PROFILE](#)

The Flexible Surface Revisited: Adsorbate-Induced Reconstruction, Homocoupling, and Sonogashira Cross-Coupling on the Au(100) Surface

Carlos Sánchez-Sánchez,^{†,‡} Francisco Yubero,[†] Agustín R. González-Elipe,[†] Leticia Feria,^{§,⊥} Javier Fernández Sanz,[§] and Richard M. Lambert^{*,†,||}

[†]Instituto de Ciencia de Materiales de Sevilla (CSIC), Americo Vespucio 49, 41092 Sevilla, Spain

[‡]EMPA, Swiss Federal Laboratories for Materials Science and Technology, Überlandstrasse 129, 8600 Dübendorf, Switzerland

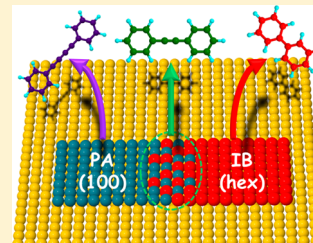
[§]Departamento de Química Física, Facultad de Química, Universidad de Sevilla, E-41012 Sevilla, Spain

^{||}Chemistry Department, Cambridge University, Cambridge CB2 1EW, United Kingdom

[⊥]Departamento de Química, Universidad Técnica Particular de Loja, P.O. Box 11-01-608, Loja, Ecuador

S Supporting Information

ABSTRACT: Phenylacetylene (PA) and iodobenzene (IB) are prototypical reactants in Sonogashira cross-coupling. Their adsorption behavior and reactivity on the Au(100) surface were studied by STM, temperature-programmed desorption and reaction, and DFT calculations that included the effect of dispersion forces. The two species exhibited very different behavior. Thus, even at 200 K, PA rearranged Au surface atoms so as to lift the hex reconstruction and adsorb in 4-fold-symmetric islands on the unreconstructed 100 surface. On the other hand, IB adsorbed on the reconstructed hex surface, again as islands, forming three different coexisting close-packed structures. The DFT results are in good accord with these findings, demonstrating the strong preference of PA and IB for the (100) and hex surfaces, respectively. Moreover, the calculated adsorption energies were in satisfactory agreement with values estimated from the desorption data. Adsorbed separately, both PA and IB underwent homocoupling, yielding diphenyl diacetylene and biphenyl, respectively; in the former case, reaction appeared to originate at island boundaries. On the well-annealed surface, coadsorbed PA and IB behaved independently, generating only products of homocoupling. However, on the Ar⁺ roughened surface, Sonogashira cross-coupling also occurred, yielding diphenyl acetylene. These findings are discussed in terms of the island-forming propensity of the reactants, amplified by the labile nature of the Au 100 surface under adsorption and the marked preference of the two reactants for different substrate structures, factors that act to inhibit the formation of a mixed adlayer and suppress reactivity. The implications for the behavior of practical Au nanoparticle catalysts are considered.



INTRODUCTION

Metal-catalyzed Sonogashira coupling reactions that lead to the formation of new C–C bonds are of strategic importance in synthetic organic chemistry. They provide a powerful and flexible method for systematically and efficiently constructing complex molecular architectures from suitably tailored building blocks and are now the most important method for preparing arylalkynes and conjugated enynes, which are key precursors in the synthesis of natural products, pharmaceuticals, and organic molecular materials.¹ Palladium species in some form constitute by far the most commonly used catalysts, although opinion remains divided in regard to the issue of homogeneous versus heterogeneous catalysis.^{2–4}

The cross-coupling of iodobenzene with phenylacetylene is a prototypical and widely studied example of Sonogashira coupling. We have demonstrated that this reaction can occur on the Au(111) surface in a vacuum environment.⁵ This was significant because there was no possibility of homogeneous chemistry having occurred under vacuum conditions, thus indicating that heterogeneous gold-catalyzed Sonogashira

coupling should be possible under practical conditions. We subsequently showed that this catalytic reaction did indeed occur heterogeneously in the solution phase at the surfaces of Au nanoparticles,⁶ as was also reported by others.⁷ Substantial particle size effects were also observed, implying significant sensitivity to the structure of the metal surface.⁸ It is therefore of interest to examine this chemistry on the Au(100) surface where the additional possibility exists for transitions between two different terminations of the metal surface.

Here, we report a fundamental study of the adsorption/desorption, structural, and reactive properties of phenylacetylene (PA) and iodobenzene (IB) on this surface, particular attention being given to mechanistic aspects, including the response of the metal surface to adsorption of the reactants. By means of STM, temperature-programmed desorption and reaction (TPD, TPR), supported by DFT calculations, it was

Received: February 6, 2014

Revised: May 15, 2014

found that the gold surface was labile, even at low temperature, and that the structure it adopted was critically dependent on the identity of the adsorbate, a striking example of “the flexible surface” proposed by Somorajai many years ago in connection with metal-catalyzed reactions.⁹ Experiment and theory show that, whereas IB adsorption on the hex-reconstructed surface is strongly preferred, in marked contrast PA lifts the reconstruction and adsorbs on the 4-fold (100) surface. The calculated adsorption energies are in satisfactory agreement with experimental estimates. Both IB and PA underwent homocoupling to yield biphenyl (BP) and diphenyl diacetylene (DPDA), respectively. When they were coadsorbed on a deliberately roughened surface, but not otherwise, Sonogashira cross-coupling to yield diphenyl acetylene (DPA) also occurred. Mechanistic aspects of the surface chemistry, including the observed effect of surface disorder, and the implications of these results for catalysis by Au nanoparticles are discussed.

■ EXPERIMENTAL METHODS

STM data were acquired with an Omicron VT-STM instrument, previously described.⁵ STM images were recorded in constant current mode and analyzed using the WSxM software.¹⁰ TPD measurements were carried out in a stainless steel ultrahigh vacuum chamber of conventional design operated at a base pressure of 2×10^{-10} mbar. It was equipped with a VG 300 quadrupole mass spectrometer for residual gas analysis and temperature-programmed desorption, a 3 grid retarding field analyzer (RFA) with integral electron gun and fluorescent screen for LEED/AES, and an ion gun for Ar⁺ sputtering. The resistively heated Au(100) single crystal was mounted on a sample holder by means of Ta clips and attached to XYZ manipulator equipped with liquid nitrogen cooling, enabling sample temperatures from ~110 to 1300 K. TPD data were taken using a linear temperature ramp (3 K/s) delivered by a programmed power supply. Repeatability of sequential TPD and TPR measurements confirmed that no significant surface contamination occurred. Adsorbate mass spectra monitored during dosing confirmed the absence of impurities. Crystal temperature was monitored via a K-type chromel–alumel thermocouple retained on the top edge of the sample with a Ta clip. The distance from the crystal front face to the collimating entrance orifice of the mass spectrometer was <10 mm; control experiments confirmed that the detected desorbing species originated entirely from the front face of the sample. The reactants (iodobenzene, phenylacetylene) and products (biphenyl, diphenyl diacetylene, diphenyl acetylene) were detected at $m/z = 204, 102, 154, 202$, and 178, respectively. The fragmentation patterns of the reactants were monitored during dosing and corresponded well with NIST data.¹¹ Approximate adsorbate exposures are specified in langmuir ($1 \text{ L} = 1.33 \times 10^{-6}$ mbar s), estimated from the total pressure during dosing, very approximate ionization gauge sensitivity factors (no data for PA and IB are available; we used data for benzene), and the corresponding mass spectrum, observed simultaneously. Accordingly, quoted exposures correspond to an upper limit with an unknown uncertainty factor.

Density Functional Theory Calculations. Surface Models and Computational Details. Two gold surfaces were modeled in this work, the unreconstructed Au(100)-(1×1) and the quasihexagonal close-packed reconstructed surface, Au(100)-hex, which is the lowest energy state under UHV conditions. The Au(100) surface was modeled by a (8×4)

supercell slab containing 128 atoms in four layers, including a vacuum of 20 Å. This model is large enough to accommodate the adsorbed species while avoiding lateral interactions. Several structures have been proposed to theoretically represent the Au(100)-hex surface, ranging from the simplest (5×1) arrangement,^{12,13} to the (5×20) reconstruction.¹⁴ To be consistent with the model adopted for the Au(100) surface, we described the hexagonal reconstruction by adding a fifth layer on top, containing 36 Au atoms, which leads to a surface density close to that of the (7×1) reconstruction. During structural optimizations, the two bottom layers were kept frozen.

Periodic DFT calculations were carried out with the Vienna ab initio Simulation Package (VASP).^{15–17} This code solves the Kohn–Sham equations for the valence electron density within a plane wave basis set and makes use of the projector augmented wave (PAW) technique to describe the interaction between the valence electrons and the atomic cores.^{18,19} The valence electrons explicitly treated are the 5d¹⁰6s¹ of Au, 2s²2p² of C, the 5s²5p⁵ of I, and the 1s¹ of H. The cutoff for the plane-wave expansion was set to 400 eV. The generalized gradient approximation (GGA) employed the Perdew, Burke, and Ernzerhof (PBE) functional.²⁰

To account for the contributions of London dispersion forces in the description of the interaction between organic molecules and metals surfaces is a challenging issue as neither LDA nor standard GGA approaches can describe nonlocal correlation effects. This leads, in general, to underestimated interaction energies. The simplest approximations, denoted as DFT-D, are simply based on the addition of atom-pairwise corrections of the form C_6R^{-6} .²¹ Out of the various, more elaborated, schemes that have been proposed to add dispersion to standard DFT approximations, the van der Waals DF method²² appears a promising approach as it is directly based on the electron density. Here, we used the recently formulated approach of Klimes et al.,²³ denoted as optB86b-vdW, because it has been shown to provide an adequate representation of the gold–water interaction;²⁴ accordingly, our discussion is based on the results of such calculations. An illustrative comparison between the results obtained by the PBE, Grimme semiempirical (PBE-D2), and the optB86b-vdW methods is provided in the Supporting Information (Table S1).

■ RESULTS AND DISCUSSION

Adsorption, Desorption, and Homocoupling of Phenylacetylene (PA). Scanning Tunneling Microscopy and Density Functional Theory. Figure 1a shows an image of the clean reconstructed Au(100)-hex surface, which accords with earlier reports.²⁵ Notice that two different domains of the hex reconstruction were imaged, with the atomic rows running either parallel or perpendicular to step edges. Adsorption of PA multilayers on this surface at 120 K resulted in fuzzy images of the type illustrated in Figure 1b, characteristic of adsorbate diffusion on surfaces.^{26–28} Annealing the sample to 200 K followed by imaging at 120 K produced islands of ordered molecules (Figure 1c), which exhibited 4-fold symmetry and were characterized by a 1.3 × 1.3 nm unit cell; the apparent molecular dimensions were commensurate with those of PA. The implication is that PA adsorption lifts the hex reconstruction, with the molecules then adsorbing on the unreconstructed (100) surface, a process that requires significant mobility of Au atoms at ~200 K; adsorbate-induced

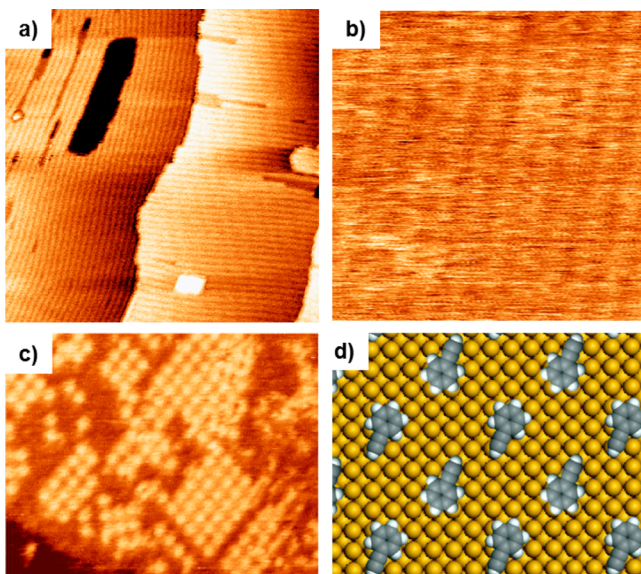


Figure 1. (a) STM image of the clean Au(100) surface. Note differently oriented domains of the hex reconstruction on adjacent terraces. $70 \text{ nm} \times 70 \text{ nm}$, $I = 0.22 \text{ nA}$, $V = -1.1 \text{ V}$, $T = 120 \text{ K}$. (b) STM image of the Au(100) surface after deposition of a PA multilayer at 120 K. $15 \text{ nm} \times 15 \text{ nm}$, $I = 1.0 \text{ nA}$, $V = 1.5 \text{ V}$, $T = 120 \text{ K}$. (c) STM image of the same sample after subsequent annealing at 200 K for 10 min. Bright features correspond to PA molecules arranged in a square array. $30 \text{ nm} \times 23.5 \text{ nm}$, $I = 0.33 \text{ nA}$, $V = 1.5 \text{ V}$, $T = 120 \text{ K}$. (d) Schematic model for a possible arrangement of the PA molecules.

low temperature diffusion of Au adatoms on Au surfaces is well documented.^{29–31}

In Figure 1c, a small patch of molecules near the bottom of the image appear with an orientation different from the other patches. This is consistent with the DFT results, which showed that the adsorption energy was not significantly dependent on the in-plane molecular orientation with respect to the metal surface,^{32,33} implying that molecule–molecule attractive interactions determine the structure of the PA overlayer. In the present case, dipole–dipole and van der Waals interactions must operate, and in cases such as the present one that involve benzenoid adsorbates on metal surfaces, adsorption-induced in-plane dipole moments can make an additional major contribution to intermolecular attractions.³⁴

A possible structure for the molecular overlayer showing the most favorable disposition of individual molecular dipoles is presented in Figure 1d; it corresponds to a density of 1 molecule per 1.7 nm^2 . This interpretation is consistent with our accurate optB86b-vdW DFT calculations (Supporting Information, Table S1), which show that the adsorption energy of PA is substantially higher on the (100) surface than on the hex surface (1.34 eV versus 1.05 eV).

After annealing to 250 K, elongated features grew out from the edges of the (100) PA islands propagating out onto (5×1) hex terraces. This behavior was even more pronounced when PA exposure was carried out at 250 K and is illustrated in Figure 2a, which shows a 4-fold symmetric domain of PA molecules on the (100) surface contiguous with some reaction product present on the hex surface and aligned with the rows of the reconstructed surface. It is noteworthy that the apparent height of these entities is $\sim 0.5 \text{ \AA}$ greater than that of the molecules within the PA island, consistent with their being located on top of the (5×1) hex surface, whereas the latter are

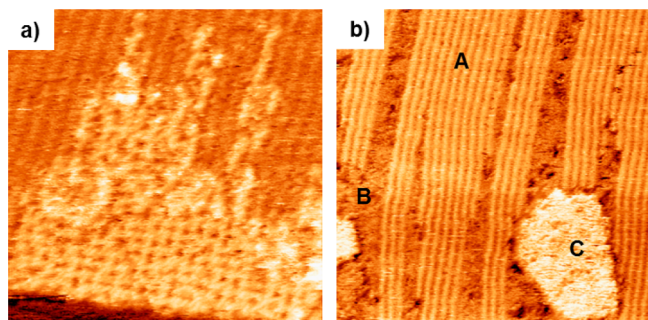


Figure 2. (a) STM image acquired at 120 K for PA molecules deposited on clean Au(100) surface at 250 K. Note the square lattice of PA molecules within the arrow-shaped island. $25.0 \text{ nm} \times 25.0 \text{ nm}$, $I = 0.22 \text{ nA}$, $V = 1.4 \text{ V}$. (b) Same surface after warming to room temperature over 12 h. Note the coexistence of three different regions: “Hex” Au(100) reconstruction (A), bare (100) surface (B), and islands of excess Au (C). $50.0 \text{ nm} \times 50.0 \text{ nm}$, $I = 0.40 \text{ nA}$, $V = 1.1 \text{ V}$.

present on the (100) surface.²⁵ Homocoupling of PA to diphenyldiacetylene (DPDA) is a plausible explanation for the reaction product: we may envisage the PA island boundary retreating as it undergoes conversion to DPDA at its edges.

Finally, annealing at $\sim 300 \text{ K}$ for 12 h resulted in the image shown in Figure 2b where three distinct areas can be distinguished. A is the originally bare (5×1) hex surface, and B is assigned to those regions from which PA has desorbed leaving behind patches of bare (100) surface; the apparent height difference between the reconstructed and unreconstructed regions is $\sim 0.5 \text{ \AA}$, which is consistent with this interpretation. C is assigned to an island of excess Au atoms expelled from the initial (5×1) hex surface as it underwent rearrangement to the (100) surface upon adsorption of PA (the hex surface contains an excess of 0.26 monolayers Au atoms relative to the unreconstructed (100) surface). The formation of these excess Au islands resulting from the hex to (100) phase transition has been previously reported by Magnussen et al.³⁵ In that study, the phase transition was induced electrochemically rather than by molecular adsorption, as in the present case. Nevertheless, the final result is the same. It is also possible that B is due to diffusing molecules; assignment to bare gold surface is prompted by the similarity between B and C. Either way, the issue is somewhat peripheral.

Temperature-Programmed Desorption and Reaction.

Figure 3 (black curve) shows thermal desorption of PA from the clean Au surface following adsorption at 115 K.

The principal low temperature feature ($\sim 180 \text{ K}$) is assigned to tilted molecules in the contact layer present at saturation coverage on an initially crowded surface after adsorption at 115 K (estimated activation energy to desorption $\sim 0.4 \text{ eV}$). The red curve was obtained after adsorption at 250 K. The principal feature at 510 K is assigned to flat-lying molecules desorbing from the partially denuded surface with an estimated activation energy of $\sim 1 \text{ eV}$, in fair agreement with the DFT result for flat-adsorbed PA (1.3 eV). Consistent with this view, the relative populations of the low temperature and high temperature states could be systematically altered by varying the adsorption temperature between 115 and 250 K. Coverage-dependent changes in the activation energy comparable to or larger than desorption for benzenoid molecules on metal surfaces are well-known³⁶ and have been associated with a change in adsorption geometry from tilted to flat-lying as coverage decreases.^{37,38}

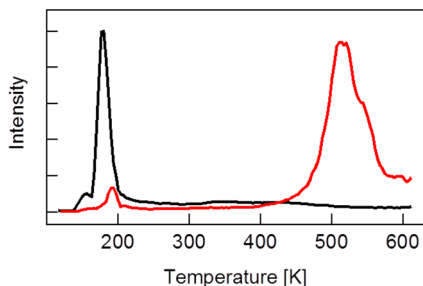


Figure 3. TPD spectra ($m/z = 102$) obtained after PA adsorption on clean Au(100), showing that population of the two states is strongly dependent on adsorption temperature. Black and red curves correspond to adsorption at 115 and 250 K, respectively. No DPDA was observed under these conditions. Estimated exposures: 3 L, black curve; 2000 L, red curve.

Adsorption, Desorption, and Homocoupling of Iodobenzene (IB). *Scanning Tunneling Microscopy and Density Functional Theory.* Very strikingly, the DFT results indicate that, whereas PA adsorbs significantly more strongly on the (100) surface than on the (5×1) hex surface, IB very strongly prefers the (5×1) hex surface according to both experiment and theory (2.16 eV versus 1.35 eV; see Table S1, Supporting Information). Also, in marked contrast with PA adsorption, STM data show that IB forms three different high density structures that coexist on the (presumably) hex surface, as shown in Figure 4a. Images were acquired after IB adsorption at 120 K followed by annealing to 250 K. In addition to the characteristic hex surface features (I), three

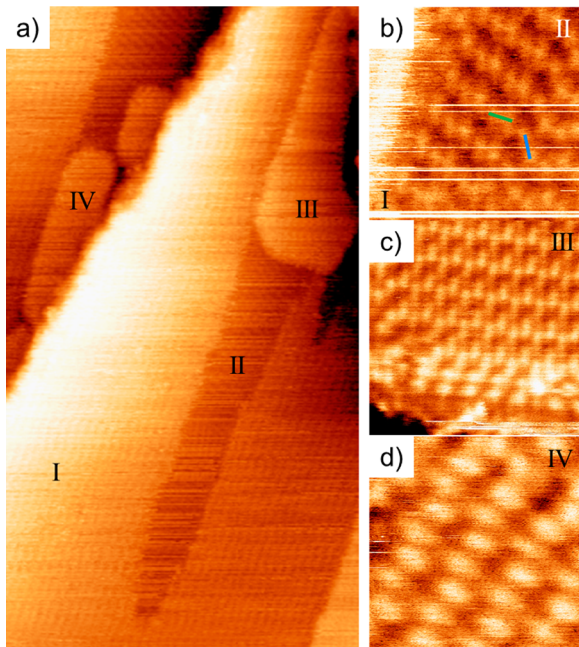


Figure 4. (a) STM images of IB adsorbed at 120 K on the clean Au-hex surface and then annealed at 250 K. Note characteristic hex rows (I) and coexistence of three different adsorbate structures: II, III, IV. $75.0 \text{ nm} \times 100.0 \text{ nm}$, $I = 0.13 \text{ nA}$, $V = 1.3 \text{ V}$. (b) Structure II presents two domains rotated by 120°, as indicated by the green and blue lines. $7.6 \text{ nm} \times 7.6 \text{ nm}$, $I = 0.2 \text{ nA}$, $V = 1.3 \text{ V}$. (c and d) Different packing structures for IB molecules due to dipole interactions. (c) $10.0 \text{ nm} \times 10.0 \text{ nm}$, $I = 0.2 \text{ nA}$, $V = 1.8 \text{ V}$. (d) $5.0 \text{ nm} \times 5.0 \text{ nm}$, $I = 0.2 \text{ nA}$, $V = 1.3 \text{ V}$. Images acquired at 120 K.

different molecular arrangements coexisted, behavior reminiscent of that reported for IB molecules on Cu(111) where the authors pointed out that "... only the least dense structure reflects the threefold symmetry of the surface."³⁹ In our case, the estimated molecular densities for the three structures II, III, and IV are 1.2, 1.2, and 1.1 molecules/nm², suggesting that energy differences between them are small. Structure II is characterized by pairs of features separated by 1 nm, and two domains are distinguishably rotated by 120° (Figure 4b). This suggests a 3-fold symmetry for the underlying surface, consistent with it being (5×1) hex and in accord with the findings of Morgenstern et al. for IB on Cu(111), who observed similar pairing of adjacent molecules of intact IB.³⁹ In all three structures, the IB molecular density is about twice that observed for PA (Figure 1), which is at least consistent with the two molecules being adsorbed on two different surfaces: high Au atomic density (5×1) in the case of IB and lower Au atomic density (100) in the case of PA. Given that the free IB molecule has a large dipole moment (1.7 D), which may well be substantially enhanced upon adsorption,⁴⁰ both II and III (Figure 4c) may be rationalized in terms of oppositely oriented adjacent IB molecules, arrangements that would have the most favorable electrostatic energy. The pairing effect, although less marked, is also visible in IV (Figure 4d).

Annealing the IB overlayer at 300 K for 10 min resulted in images of the type illustrated in Figure 5a and in more detail in

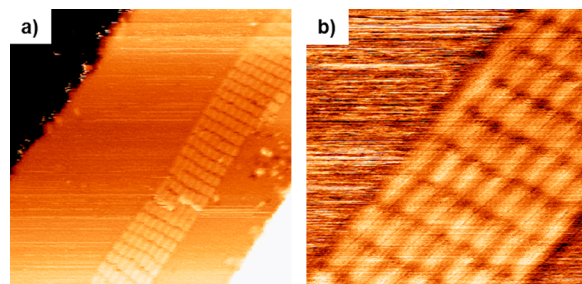


Figure 5. (a) STM image of the surface after annealing at 300 K for 10 min showing formation of elongated structures ascribed to BP molecules resulting from the Ullmann coupling of IB. $50.0 \text{ nm} \times 50.0 \text{ nm}$, $I = 0.3 \text{ nA}$, $V = 1.2 \text{ V}$. (b) Magnified image. $15.0 \text{ nm} \times 15.0 \text{ nm}$, $I = 1.0 \text{ nA}$, $V = 0.3 \text{ V}$. Images acquired at 120 K.

Figure 5b. The dimensions of the well-ordered and aligned species accord well with those of biphenyl (BP) formed by Ullman coupling of pairs of IB molecules.

Temperature-Programmed Desorption and Reaction. Iodobenzene desorption following adsorption at 120 K is shown as the black curve in Figure 6; the minor peak at ~ 170 K is due to a small amount of multilayer, the ~ 220 K feature is again ascribed to contact layer molecules on the initially crowded surface, and, as with PA, the higher temperature peaks are ascribed to more strongly adsorbed molecules lying flat on the denuded surface; that is, these are the species to which the DFT calculations refer. Again, as in the case of PA, the relative amounts of molecules in the two states could be varied by changing the adsorption temperature; the red curve in Figure 6 illustrated the effect of adsorbing IB at 250 K.

The highest temperature peak, corresponding to the lowest molecular coverage, yields an estimated desorption energy of ~ 1.8 eV, which is to be compared to the DFT value of 2.1 eV for a flat-lying IB molecule on an otherwise bare 5×1-hex surface. The corresponding value calculated for the 4-fold

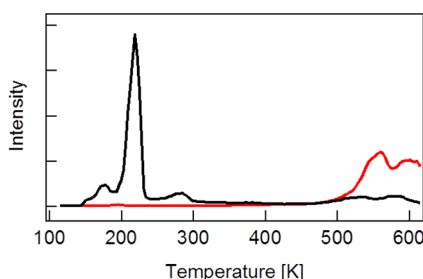


Figure 6. TPD spectra ($m/z = 204$) for IB adsorbed on clean Au(100) surface. Black and red curves correspond to adsorption at 120 and 250 K, respectively. As with PA (Figure 3), the relative population of the high and low temperature states was strongly dependent on adsorption temperature. Estimated exposures: ≤ 1300 L, black curve; ≤ 5400 L, red curve.

symmetric 100 surface is much lower, 1.3 eV (Table S1, Supporting Information). Thus, theory indicates that, in contrast to PA, IB should strongly prefer the 5×1 -hex surface, which is consistent with our rationalization of the STM data in terms of IB adsorption on the 5×1 -hex surface.

In ref 5, following adsorption at 90 K, only a single peak was reported at ~ 310 K for both IB and PA desorbing from Au(111), intermediate between the low temperature and high temperature desorption regimes observed here. In the present case, ~ 200 K desorption dominated when adsorption was carried out at 120 K, extensive population of the high temperature state only occurring when adsorption was carried out at 250 K. This implies the existence of an activation barrier to the transition from low temperature to high temperature states in the present case, absent in the case of Au(111).

Sonogashira Cross-Coupling of PA with IB. Initial experiments indicated that TPR following sequential adsorption of PA and IB resulted in the formation of all three possible products that can result from homo- and cross-coupling, as shown in Scheme 1.

However, sequential dosing of PA and IB proved to be unsatisfactory due to the “stickiness” of both molecules within the vacuum system (long pump out times between dosing one species and then the other); the problem was exacerbated by displacement of one molecule from the walls of the equipment when the second molecule was introduced. Instead, we adopted a simultaneous dosing methodology using a mixture of liquid PA and IB in the sample reservoir. The vapor pressures of IB and PA at room temperature are approximately equal. Thus, if the two species form an approximately ideal solution that therefore approximately follows Raoult’s law, a 1:1 liquid mixture should generate a $\sim 1:1$ composition in the vapor

phase. In practice, this approach was very satisfactory and produced reliably reproducible results. Mass spectra of the vapor indicated approximately equal pressures of the two molecules and no detectable amounts of any other species. Likewise, subsequent TPD of the mixed adsorption layer showed that the uptake of both adsorbates was indeed about the same.

On the smooth annealed Au surface, coadsorbed IB and PA both underwent homocoupling to yield BP and DPDA, respectively, but no Sonogashira cross-coupling to form DPA was detected. STM images showed domains of ordered IB together with regions consisting of disordered molecules that could be PA (see Figure S1, Supporting Information); IB molecules always formed highly ordered structures under these conditions, as illustrated in Figure 4a and b. However, when the surface was subjected to Ar^+ sputtering before reaction, all three products were observed. Representative TPR results obtained after coadsorption of PA+IB at 180 K on a sputtered surface are shown in Figure 7. DPDA was formed from PA in both the low

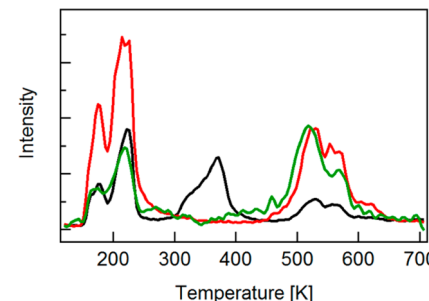
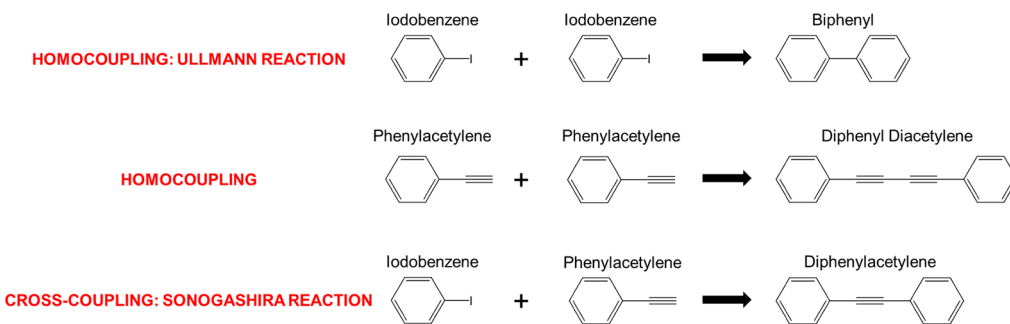


Figure 7. TPR spectra for multilayer coverage of IB and PA adsorbed at 180 K on heavily sputtered Au(100) surface from a 1:1 mixed solution. Black, red, and green curves correspond to BP ($m/z = 154$), DPDA ($m/z = 202$), and DPA ($m/z = 178$) $\times 10$ desorption, respectively. There was no possibility of an experimental artifact involving cross-talk between the m/z 188 (DPA) and 202 (DPDA) channels of the QMS output, and there are no fragment ions of DPDA that could be mistaken for DPA parent ion. The similarities in the profiles are to be taken at face value. See text.

temperature (~ 200 K) and the high temperature regimes (550 K). BP, resulting from homocoupling of IB, was also formed in the low temperature and high temperature regimes, accompanied by significant additional BP formation at intermediate temperatures (~ 350 K). The results indicate that for DPA and DPDA, reaction occurs in the same temperature range as that for reactant desorption. The implication is that for PA and IB, desorption and reaction are in competition in both the low

Scheme 1. Scheme of the Different Reactions That May Take Place for the Codosing of IB and PA



temperature and the high temperature regimes, the appearance of gaseous products being reaction rate-limited. A similar argument holds for BP desorption, except in this case there is an additional peak at intermediate temperature (~ 380 K), implying that some phenyl radicals liberated in the low temperature regime survive to dimerize at higher temperature. Interestingly, the temperature we observe for this process is similar to that reported by Syomin et al. for the desorption of both reactively formed BP and BP preadsorbed on Au(111); that is, reactively formed BP appears in the gas phase as a result of a desorption rate-limited process.⁴¹ It thus appears that a different reaction mechanism operates for BP formation in the intermediate temperature regime.

Now, however, Sonogashira cross-coupling also occurred, forming diphenyl acetylene (DPA) in both the high and the low temperature regimes.

These observations may be plausibly rationalized in terms of the following (admittedly simplified) model. STM shows that both PA and IB exhibit strong island-forming tendencies, the two molecules preferring different Au substrate structures. Molecules at island peripheries are reactive; those within the island are not. Thus, homocoupling can always take place at the boundaries of PA and IB islands, yielding DPDA and BP, as observed, whereas Sonogashira coupling can only occur when the two types of islands are sufficiently proximate. When the islands are large (smooth surface, wide terraces), the number of proximate PA and IB molecules is necessarily small and Sonogashira coupling is suppressed. When the molecular islands are small (sputtered surface), PA-IB proximity is proportionally greater and Sonogashira coupling occurs to an extent comparable to that of the two homocoupling reactions. (STM studies of the effects of Ar⁺ bombardment on the Au(100) surface showed that single vacancies were formed initially; with increasing ion dose dislocations and eventually a high density of rectangular vacancy, islands were generated (<10 nm), consistent with the above proposal.^{42,43})

It is noteworthy that all three types of coupling chemistry take place over such wide temperature regimes; according to our hypothesis, the implication is that both tilted and flat-lying molecules are reactive. Similar behavior has been reported in the case of acetylene coupling on Pd(111) where trimerization to benzene occurs in two distinct temperature regimes (240 and 520 K) associated with high and low reactant coverages, respectively.⁴⁴

On Au(111), the opposite behavior was reported.⁵ Sonogashira coupling of PA and IB did not occur on the smooth surface but did occur on the roughened surface. On that surface, organic adsorbates are known to nucleate as islands in the elbows of the herringbone reconstruction.^{45–47} Therefore, small patches of PA and IB could be nucleated immediately in close proximity to each other leading to Sonogashira coupling at their boundaries on the smooth surface. Ar⁺ bombardment of Au(111) presumably reduced the terrace dimensions to the extent that the nucleation of proximate island of PA and IB was prevented, hence no Sonogashira coupling. This suggestion is at least consistent with STM studies of ion bombarded Au(111) surfaces, which exhibit a high density of vacancy islands (~ 10 nm) within most of which the herringbone reconstruction appears to have been quenched.^{48–50}

In the present case, the island-forming propensity of the reactants is amplified by the labile nature of the Au 100 surface under adsorption and the marked preference of the two

reactants for different substrate structures. This inhibits the formation of a mixed adlayer and suppresses reactivity. Accordingly, from the viewpoint of catalysis by Au NPs, one might anticipate marked particle shape effects, determined by the preponderance or otherwise of 100 facets, ranging from 100% in the case of nanocubes to $\sim 0\%$ in the case of 111-oriented nanoplates, with spherical particles, cuboctahedra, icosahedra, branched particles, and nanobelts exhibiting intermediate behavior. As Au nanoparticles may be synthesized in all of these shapes,⁵¹ an interesting prospect presents itself. The idea that metal surfaces may be “flexible” under conditions of catalytic reaction is not new, having been proposed many years ago by Somorjai and reviewed by him more recently.⁹ The case of Au appears to be especially pertinent, given the high level of current interest in catalysis by Au nanoparticles, including effects of Au particle shape in catalysis of organic reactions.⁵² A recent experimental and theoretical study of Sonogashira coupling of PA with *p*-iodoanisole using precisely defined Au₂₅ clusters nicely illustrates the importance of adsorption site structure, although the authors were unaware of the possibility that PA could have restructured the Au cluster. In situ EXAFS measurements on nanoparticle practical catalysts could in principle be used to address directly this potentially important issue.⁵³

CONCLUSIONS

(1) Phenylacetylene and iodobenzene behave very differently on the Au(100) surface, exhibiting strong preferences for the unreconstructed and hex-reconstructed substrate structures, respectively.

(2) DFT calculations that take explicit account of dispersion forces are consistent with observation, and the calculated adsorption energies are in satisfactory agreement with experimental estimates.

(3) When coadsorbed, PA and IB react independently on the smooth well-annealed surface yielding only the products of homocoupling, a tendency that is probably amplified by their preferences for different substrate structures, thus limiting interaction between them to the boundaries of proximate islands.

(4) On the roughened surface, where island growth is necessarily limited and interisland contact is enhanced, Sonogashira cross-coupling occurred, underling the likely importance of spatial distribution of reactants in this area of catalytic chemistry.

ASSOCIATED CONTENT

Supporting Information

Table S1: Effect of the dispersion on calculated adsorption energies. Figure S1: STM images after IB+PA codosing. This material is available free of charge via the Internet at <http://pubs.acs.org>.

AUTHOR INFORMATION

Corresponding Author

*E-mail: rml1@cam.ac.uk

Notes

The authors declare no competing financial interest.

ACKNOWLEDGMENTS

We thank the Junta de Andalucía (Projects P12-FQM-2265, TEP-08067, and P10-FQM-6900) and the Ministry of Science

and Innovation (Projects CONSOLIDER CSD2008-00023, MAT2010-21228, and MAT2010-18447) for financial support.

REFERENCES

- (1) Chinchilla, R.; Najera, C. Recent Advances in Sonogashira Reactions. *Chem. Soc. Rev.* **2011**, *40*, 5084.
- (2) Ellis, P. J.; Fairlamb, I. J. S.; Hackett, S. F. J.; Wilson, K.; Lee, A. F. Evidence for the Surface-Catalyzed Suzuki–Miyaura Reaction over Palladium Nanoparticles: An Operando XAS Study. *Angew. Chem., Int. Ed.* **2010**, *49*, 1820.
- (3) Le Bars, J.; Specht, U.; Bradley, J. S.; Blackmond, D. G. A Catalytic Probe of the Surface of Colloidal Palladium Particles Using Heck Coupling Reactions. *Langmuir* **1999**, *15*, 7621.
- (4) Cwik, A.; Hell, Z.; Figueras, F. A Copper-Free Sonogashira Reaction Using a Pd/MgLa Mixed Oxide. *Tetrahedron Lett.* **2006**, *47*, 3023.
- (5) Kanuru, V. K.; Kyriakou, G.; Beaumont, S. K.; Papageorgiou, A. C.; Watson, D. J.; Lambert, R. M. Sonogashira Coupling on an Extended Gold Surface in Vacuo: Reaction of Phenylacetylene with Iodobenzene on Au(111). *J. Am. Chem. Soc.* **2010**, *132*, 8081.
- (6) Beaumont, S. K.; Kyriakou, G.; Lambert, R. M. Identity of the Active Site in Gold Nanoparticle-Catalyzed Sonogashira Coupling of Phenylacetylene and Iodobenzene. *J. Am. Chem. Soc.* **2010**, *132*, 12246.
- (7) Corma, A.; Juarez, R.; Boronat, M.; Sanchez, F.; Iglesias, M.; Garcia, H. Gold Catalyzes the Sonogashira Coupling Reaction without the Requirement of Palladium Impurities. *Chem. Commun.* **2011**, *47*, 1446.
- (8) Kyriakou, G.; Beaumont, S. K.; Humphrey, S. M.; Antonetti, C.; Lambert, R. M. Sonogashira Coupling Catalyzed by Gold Nanoparticles: Does Homogeneous or Heterogeneous Catalysis Dominate? *ChemCatChem* **2010**, *2*, 1444.
- (9) Somorjai, G. A. The Flexible Surface: New Techniques for Molecular Level Studies of Time Dependent Changes in Metal Surface Structure and Adsorbate Structure During Catalytic Reactions. *J. Mol. Catal. A: Chem.* **1996**, *107*, 39.
- (10) Horcas, I.; Fernandez, R.; Gomez-Rodriguez, J. M.; Colchero, J.; Gomez-Herrero, J.; Baro, A. M. WSxM: A Software for Scanning Probe Microscopy and a Tool for Nanotechnology. *Rev. Sci. Instrum.* **2007**, *78*, 013705.
- (11) <http://webbook.nist.gov/chemistry/>.
- (12) Feng, Y. J.; Bohnen, K. P.; Chan, C. T. First-Principles Studies of Au(100)-hex Reconstruction in an Electrochemical Environment. *Phys. Rev. B* **2005**, *72*, 125401.
- (13) Jacob, T. Potential-Induced Lifting of the Au(100)-Surface Reconstruction Studied with DFT. *Electrochim. Acta* **2007**, *52*, 2229–2235.
- (14) Havu, P.; Blum, V.; Havu, V.; Rinke, P.; Scheffler, M. Large-Scale Surface Reconstruction Energetics of Pt(100) and Au(100) by All-Electron Density Functional Theory. *Phys. Rev. B* **2010**, *82*, 161418R.
- (15) Kresse, G.; Hafner, J. Ab Initio Molecular Dynamics for Liquid Metals. *Phys. Rev. B* **1993**, *47*, 558.
- (16) Kresse, G.; Hafner, J. Ab Initio Molecular Dynamics for Open-Shell Transition Metals. *Phys. Rev. B* **1993**, *48*, 13115.
- (17) Kresse, G.; Hafner, J. Ab Initio Molecular-Dynamics Simulation of the Liquid-Metal–Amorphous–Semiconductor Transition in Germanium. *Phys. Rev. B* **1994**, *49*, 14251.
- (18) Blochl, P. E. Projector Augmented-Wave Method. *Phys. Rev. B* **1994**, *50*, 17953.
- (19) Kresse, G.; Joubert, D. From Ultrasoft Pseudopotentials to the Projector Augmented-Wave Method. *Phys. Rev. B* **1999**, *59*, 1758.
- (20) Perdew, J. P.; Burke, K.; Ernzerhof, M. Generalized Gradient Approximation Made Simple. *Phys. Rev. Lett.* **1996**, *77*, 3865.
- (21) Grimme, S. Semiempirical GGA-Type Density Functional Constructed with a Long-Range Dispersion Correction. *J. Comput. Chem.* **2006**, *27*, 1787–1799.
- (22) Dion, D.; Rydberg, H.; Schröder, E.; Langreth, D. C.; Lundqvist, B. I. Van der Waals Density Functional for General Geometries. *Phys. Rev. Lett.* **2004**, *92*, 246401.
- (23) Klimeš, J.; Bowler, D. R.; Michaelides, A. Van der Waals Density Functionals Applied to Solids. *Phys. Rev. B* **2011**, *83*, 195131.
- (24) Nadler, R.; Sanz, J. F. Effect of Dispersion Correction on the Au(1 1 1)-H₂O Interface: a First-Principles Study. *J. Chem. Phys.* **2012**, *137*, 114709.
- (25) Hernán, O. S.; Gallego, J. M.; Vázquez de Parga, A. L.; Miranda, R. Initial Growth of Fe on Au(100): Preferential Nucleation, Place Exchange and Enhanced Mass Transport. *Appl. Phys. A: Mater. Sci. Process.* **1998**, *66*, S1117–S1120.
- (26) Lanzilotto, V.; Sanchez-Sanchez, C.; Bavdek, G.; Cvetko, D.; Lopez, M. F.; Martin-Gago, J. A.; Floreano, L. Planar Growth of Pentacene on the Dielectric TiO₂(110) Surface. *J. Phys. Chem. C* **2011**, *115*, 4664–4672.
- (27) Sanchez-Sanchez, C.; Lanzilotto, V.; Gonzalez, C.; Verdini, A.; de Andres, P. L.; Floreano, L.; Lopez, M. F.; Martin-Gago, J. A. Weakly Interacting Molecular Layer of Spinning C₆₀ Molecules on TiO₂ (110) Surfaces. *Chem.—Eur. J.* **2012**, *18*, 7382–7387.
- (28) Sánchez-Sánchez, C.; Martínez, J. I.; Lanzilotto, V.; Biddau, G.; Gómez-Lor, B.; Pérez, R.; Floreano, L.; López, M. F.; Martín-Gago, J. A. Chemistry and Temperature-Assisted Dehydrogenation of C₆₀H₃₀ Molecules on TiO₂(110) Surfaces. *Nanoscale* **2013**, *5*, 11058.
- (29) Cyganik, P.; Buck, M.; Strunskus, T.; Shaporenko, A.; Witte, G.; Zharnikov, M.; Wöll, C. Influence of Molecular Structure on Phase Transitions: A Study of Self-Assembled Monolayers of 2-(Aryl)-ethane Thiols. *J. Phys. Chem. C* **2007**, *111*, 16909–16919.
- (30) Baber, A. E.; Jensen, S. C.; Iski, E. V.; Sykes, E. C. H. Extraordinary Atomic Mobility of Au{111} at 80 K: Effect of Styrene Adsorption. *J. Am. Chem. Soc.* **2006**, *128*, 15384–15385.
- (31) Kautz, N. A.; Kandel, S. A. Alkanethiol/Au(111) Self-Assembled Monolayers Contain Gold Adatoms: Scanning Tunneling Microscopy Before and After Reaction with Atomic Hydrogen. *J. Am. Chem. Soc.* **2008**, *130*, 6908–6909.
- (32) Soukopp, A.; Glöckler, K.; Kraft, P.; Schmitt, S.; Sokolowski, M.; Umbach, E.; Mena-Osteritz, E.; Bäuerle, P.; Hädicke, E. Superstructure Formation of Large Organic Adsorbates on a Metal Surface: A Systematic Approach Using Oligothiophenes on Ag(111). *Phys. Rev. B* **1998**, *58*, 13882.
- (33) Grimley, T. B. The Indirect Interaction Between Atoms or Molecules Adsorbed on Metals. *Proc. Phys. Soc.* **1967**, *90*, 751.
- (34) Vaughan, O. P. H.; Alavi, A.; Williams, F. J.; Lambert, R. M. Dipole Amplification: A Principle for the Self-Assembly of Asymmetric Monomers on Metal Surfaces. *Angew. Chem., Int. Ed.* **2008**, *47*, 2422.
- (35) Magnussen, O. M.; Hotlos, J.; Behm, R. J.; Batina, N.; Kolb, D. M. An In-Situ Scanning Tunneling Microscopy Study of Electrochemically Induced “hex” – (1×1) Transitions on Au(100) Electrodes. *Surf. Sci.* **1993**, *296*, 310.
- (36) Schießer, A.; Hörtz, P.; Schäfer, R. Thermodynamics and Kinetics of CO and Benzene Adsorption on Pt(111) Studied with Pulsed Molecular Beams and Microcalorimetry. *Surf. Sci.* **2010**, *604*, 2098–2105.
- (37) Netzer, F. P.; Rangelov, G. The Orientation of Pyridine on Rh(111). *Surf. Sci.* **1990**, *225*, 260–266.
- (38) Lee, J.-G.; Ahner, J.; Yates, J. T. The Adsorption Conformation of Chemisorbed Pyridine on the Cu(110) Surface. *J. Chem. Phys.* **2001**, *114*, 1414.
- (39) Morgenstern, K.; Hla, S. W.; Rieder, K.-H. Coexisting Superstructures of Iodobenzene on Cu(1 1 1) Near Saturation Coverage. *Surf. Sci.* **2003**, *523*, 141.
- (40) Vaughan, O. P. H.; Alavi, A.; Williams, F. J.; Lambert, R. M. Dipole Amplification: A Principle for the Self-Assembly of Asymmetric Monomers on Metal Surfaces. *Angew. Chem., Int. Ed.* **2008**, *47*, 2422.
- (41) Syomin, D.; Koel, B. E. Adsorption of Iodobenzene (C₆H₅I) on Au(111) Surfaces and Production of Biphenyl (C₆H₅–C₆H₅). *Surf. Sci.* **2001**, *490*, 265.
- (42) Rodriguez de la Fuente, O.; Gonzalez-Barrio, M. A.; Navarro, V.; Pabón, B. M.; Palacio, I.; Mascaraque, A. Surface Defects and Their Influence on Surface Properties. *J. Phys.: Condens. Matter.* **2013**, *25*, 484008.

- (43) Rodriguez de la Fuente, O.; Gonzalez-Barrio, M. A.; Rojo, J. M. Ion Bombardment of Reconstructed Metal Surfaces: From Two-Dimensional Dislocation Dipoles to Vacancy Pits. *Phys. Rev. B* **2001**, *63*, 085420.
- (44) Tysoe, W. T.; Nyberg, G. L.; Lambert, R. M. Low Temperature Catalytic Chemistry of the Pd(111) Surface: Benzene and Ethylene from Acetylene. *J. Chem. Soc., Chem. Commun.* **1983**, *11*, 623.
- (45) Écija, D.; Otero, R.; Sánchez, L.; Gallego, J. M.; Wang, J.; Alcamí, M.; Martín, F.; Martín, N.; Miranda, R. Crossover Site-Selectivity in the Adsorption of the Fullerene Derivative PCBM on Au(111). *Angew. Chem., Int. Ed.* **2007**, *46*, 7874.
- (46) Yokoyama, T.; Yokoyama, S.; Kamikado, T.; Okuno, Y.; Mashiko, S. Selective Assembly on a Surface of Supramolecular Aggregates with Controlled Size and Shape. *Nature* **2001**, *413*, 619.
- (47) Böhringer, M.; Morgenstern, K.; Schneider, W.-D.; Berndt, R.; Mauri, F.; De Vita, A.; Car, R. Two-Dimensional Self-Assembly of Supramolecular Clusters and Chains. *Phys. Rev. Lett.* **1999**, *83*, 324.
- (48) Repain, V.; Berroir, J. M.; Rousset, S.; Lecoeur, J. Interaction Between Steps and Reconstruction on Au(111). *Europhys. Lett.* **1999**, *47*, 435–441.
- (49) Chandra Bose, A.; Yoshitake, M. Pattern Formation Induced by Ar+ Sputtering on Au(111). *Appl. Surf. Sci.* **2005**, *241*, 174–178.
- (50) Lang, A.; Quate, C. F.; Nogami, J. Initial Stages of Sputtering on Au(111) as Seen by Scanning Tunneling Microscopy. *Appl. Phys. Lett.* **1991**, *59*, 1696.
- (51) Nguyen, D. T.; Kim, D. J.; Kim, K.-S. Controlled Synthesis and Biomolecular Probe Application of Gold Nanoparticles. *Micron* **2011**, *42*, 207.
- (52) Watt, J.; Cheong, S.; Tilley, R. D. How to Control the Shape of Metal Nanostructures in Organic Solution Phase Synthesis for Plasmonics and Catalysis. *Nano Today* **2013**, *8*, 198–215.
- (53) Li, G.; Jiang, D.-E.; Liu, C.; Yu, C.; Jin, R. Oxide-Supported Atomically Precise Gold Nanocluster for Catalyzing Sonogashira Cross-Coupling. *J. Catal.* **2013**, *306*, 177–183.